

Eco-Friendly and Systematic Study for Synthesis of $\text{La}^{3+}/\alpha\text{-Al}_2\text{O}_3$ Nanoparticles: Antibacterial Activity Against Pathogenic Microbial Strains

This article was published in the following Dove Press journal:
International Journal of Nanomedicine

Mohammad Hasan Moshafi¹
Mehdi Ranjbar^{2,3}
Ghazaleh Ilbeigi⁴

¹Neuroscience Research Center, Institute of Neuropharmacology, Kerman University of Medical Sciences, Kerman, Iran; ²Food Drug and Cosmetics Safety Research Center Kerman University of Medical Sciences, Kerman, Iran;

³Pharmaceutics Research Center, Institute of Neuropharmacology, Kerman University of Medical Sciences, Kerman, Iran; ⁴Student Research Committee, Kerman University of Medical Sciences, Kerman, Iran

Purpose: In this study, for the first time, new nanoparticles of $\text{La}^{3+}/\alpha\text{-Al}_2\text{O}_3$ were synthesized with the ultrasonic-assisted hydrothermal method in the presence of honey as an eco-friendly and natural reagent.

Methods: The as-synthesized $\text{La}^{3+}/\alpha\text{-Al}_2\text{O}_3$ nanoparticles were characterized using scanning electron microscopy (SEM), transition electron microscopy (TEM), X-ray diffraction spectroscopy (XRD), energy dispersive X-ray (EDX), UV-visible spectroscopy, and Fourier transform infrared spectroscopy (FTIR) techniques. In this work, we report optimum conditions to synthesize $\text{La}^{3+}/\alpha\text{-Al}_2\text{O}_3$ nanoparticles as novel material and as a candidate for antibacterial activity in antibacterial drugs.

Results and Conclusion: The XRD and SEM micrograph results demonstrate the formation of pure $\text{La}^{3+}/\alpha\text{-Al}_2\text{O}_3$ nanoparticles with a particle size in the range of 30–80 nm. The synthesis parameters were systematically examined using analysis of variance (ANOVA) through $2k^{-1}$ factorial design, and the factors were an assay for product optimization. Various factors such as hydrothermal time, temperature, ultrasound irradiation and interaction between these factors were investigated on the product size of the products. To investigate antibacterial activity of the $\text{La}^{3+}/\alpha\text{-Al}_2\text{O}_3$ nanoparticles with the minimum inhibitory concentration (MIC) method, different dilutions of nanoparticles as 64, 32, 16, 8, 4, 2, 1 and 0.5 $\mu\text{g}/\text{mL}$ were dissolved in dimethyl sulfoxide and diluted using distilled water and added to the Mueller-Hinton agar medium containing *Escherichia coli*, *Klebsiella pneumonia*, *Pseudomonas aeruginosa* and *Serratia marcescens* as gram-negative bacteria and *Bacillus subtilis*, *Staphylococcus aureus*, *S. epidermidis* and *Micrococcus luteus* as gram-positive bacteria.

Keywords: ultrasound-assisted hydrothermal method, antibacterial activity, $\text{La}^{3+}/\alpha\text{-Al}_2\text{O}_3$ NPs, nanocomposites

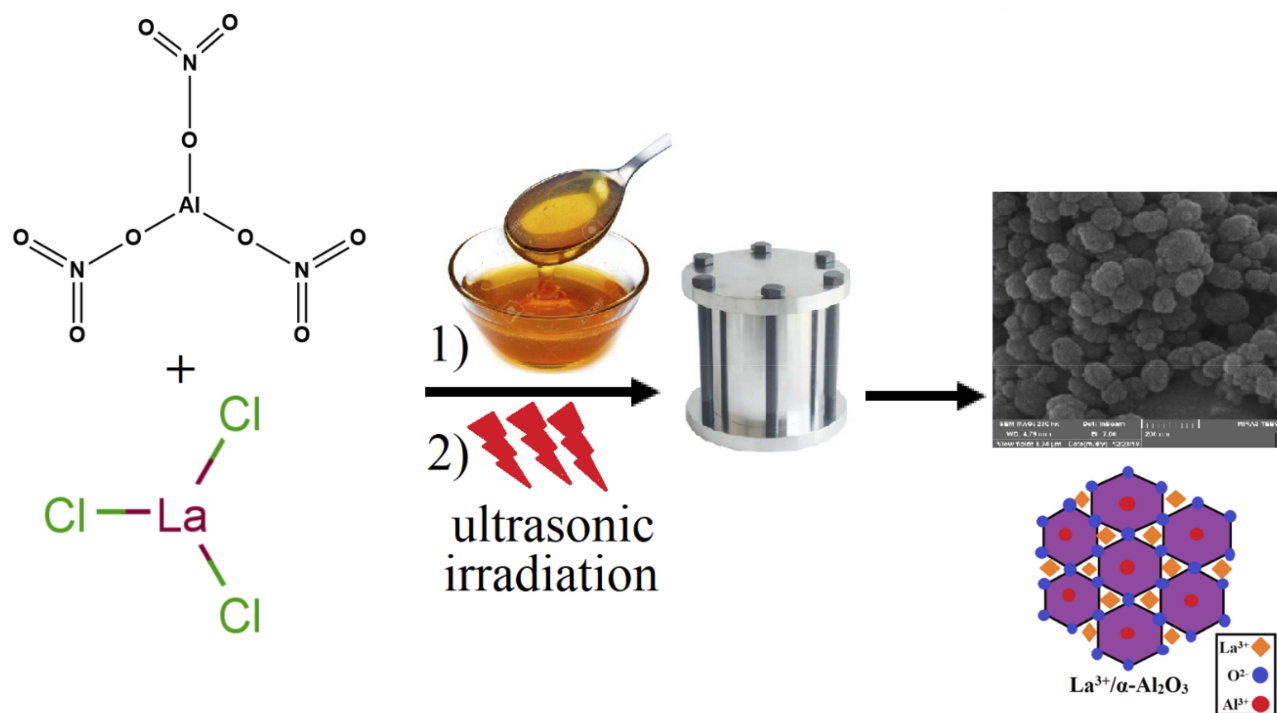
Introduction

Nowadays, antibacterial and antioxidant activity are among the effective researches in nanotechnology.¹ Honey consists of 80–85% carbohydrate (mainly glucose and fructose), 15–17% water, 0.1–0.4% protein, 0.2% ash, and minor quantities of amino acids, enzymes, and vitamins as well as other substances like phenolic antioxidants. The fructose percentage is approximately 32.56–38.2% and the glucose percentage approximately 28.54–31.3% and, as the major carbohydrates present in honey, act as natural stabilizers and a capping agent in the wet synthesis of nanoparticles.² In today's modern life human beings have been exposed to the influence of different bacteria, tissue respiration, chemical reaction, magnetic waves and other factors

Correspondence: Mehdi Ranjbar
Pharmaceutics Research Center, Kerman University of Medical Sciences, P.O. Box: 76175-493, Kerman 76169-11319, Iran
Tel +98-34-31325241
Fax +98-34-31325003
Email Mehdi.Ranjbar@kmu.ac.ir

which cause the production of antioxidants in the body;³ therefore the importance of dual-substance material is felt more than ever before.⁴ Literature searches prove that many methods such as the sol-gel method and coprecipitation method which are earlier and easier have been successfully used to synthesize nanoparticles,⁵⁻⁹ but most of these methods are difficult and costly and use harmful chemicals.^{10,11} La^{3+} as a lanthanide element has various active biological¹² and biomedical¹³ applications owing to its unique 4f electron configuration.¹⁴ As a corollary, the concept of “green nanotechnology” emerged with the green synthesis of nanoparticles commencing a new period in nanotechnology and chemistry and having a significant advance in biomedical applications, such as targeted¹⁵ drug delivery,^{16,17} gene delivery,¹⁸ hyperthermia,¹⁹ photothermal therapy,²⁰ bioimaging,²¹ and biosensors.²² The hydrothermal synthesis method includes many advantages such as the solubility of oxides in solutions higher than water,²³ the ability to synthesize crystals which are unstable near the melting point and also the ability to synthesize metal oxide crystals with high quality.²⁴ Among the most promising of the new antimicrobial agents’ metal oxide nanoparticles have been shown to have high potential antibacterial activity in a large number of studies.²⁵⁻²⁸ Different researchers have indicated that Al_2O_3 contamination with

other antioxidant metals improves photocatalytic activity and stability in $\alpha\text{-Al}_2\text{O}_3$ structural phase,²⁹⁻³¹ and leads to shifted emission peaks toward visible light, in addition to the presence of an auxiliary species, which can be effective in reducing the time of complete elimination of bacteria in the presence of ultraviolet light.^{32,33} Nanocomposites with the use of ultrafine particles have wide applications in antibacterial properties.³⁴ The effects of nanoparticles on cells of living organisms depend on the diameter, size and shape of nanoparticles.³⁵ In this study, we introduced the synthesis of $\text{La}^{3+}/\alpha\text{-Al}_2\text{O}_3$ nanoparticles with honey used as biocompatible capping agents using the ultrasound assisted hydrothermal method. Scheme 1 shows a summary of the experimental route for the synthesis of the $\text{La}^{3+}/\alpha\text{-Al}_2\text{O}_3$ NPs. The final products were characterized by different techniques such as XRD, SEM, TEM, FT-IR, UV-vis, and BET analysis. The antibacterial activity of the $\text{La}^{3+}/\alpha\text{-Al}_2\text{O}_3$ nanoparticles was investigated on *E. coli* PTCC 1330, *K. pneumoniae* PTCC 1053, *S. marcescens* PTCC1621, *P. aeruginosa* PTCC1074, *S. aureus* PTCC. 1112, *M. luteus* PTCC. 1110, and *B. subtilis* PTCC. 1023. The bacteria ranged from 64 $\mu\text{g}/\text{mL}$ up to 0.5 $\mu\text{g}/\text{mL}$. The results show that the $\text{La}^{3+}/\alpha\text{-Al}_2\text{O}_3$ nanoparticles are well capable of inhibiting the growth of the pathogenic microbial strains.



Scheme 1 Summary of experimental route for the synthesis of the $\text{La}^{3+}/\alpha\text{-Al}_2\text{O}_3$ NPs.

Experimental

Materials

All the primitives used in this work such as $\text{Al}(\text{NO}_3)_3 \cdot 9\text{H}_2\text{O}$, Lanthanum(III) chloride hydrate 99.9% as the starting precursor, and NaOH and liquor ammonia solution containing 25% ammonia (NH_3) were purchased from Merck and had analytical grade without additional purification. The deionized water used in this research work was provided in the laboratory.

Characterization

We used an automatic ultrasonic generator device (Sonicator 3000; Bandeline, MS 72, Germany), equipped with a converter/transducer and titanium oscillator (horn), 12.5 mm in diameter, operating at 20 kHz with a maximum power output of 400 W for ultrasonic irradiation. For the hydrothermal method, the reactions were carried out in the steel autoclave with a diameter of 25 cm. The XRD patterns of products were recorded with a Rigaku D-max C III, X-ray diffractometer using Ni-filtered Cu-K α radiation. For the investigation of morphological properties and particle size distribution scanning electron microscopy (SEM) images were obtained with a Philips XL-30 ESEM equipped with an energy dispersive X-ray spectroscopy (EDX) under the acceleration voltage of 100kv. The transmission electron microscope (TEM, JEM1200EX, JEOL). The Fourier-transform infrared spectroscopy (FT-IR) spectra were recorded by a Shimadzu Varian 4300 spectrophotometer in KBr pellets in the range of 400–4000 cm^{-1} . The surface area, porosity, pore size and volume properties of the nanostructure were studied by a Brunauer-Emmett-Teller (BET), and N_2 adsorption-desorption isotherms of the samples were recorded by using Belsorp II-BEL equipment (BEL Japan Inc., Osaka, Japan). Gram-positive and four Gram-negative standard bacterial strains were purchased from the Iranian Scientific and Industrial Research Organization.

Preparation of $\text{La}^{3+}/\alpha\text{-Al}_2\text{O}_3$ Nanoparticles

In this study at first 15 mL ammonia was mixed with distilled water (DW) 1: 1 ratio then 0.41 g $\text{Al}(\text{NO}_3)_3 \cdot 9\text{H}_2\text{O}$ was added to the above solution. In another beaker 0.046 mol of Lanthanum(III) chloride was dissolved in 20 mL of deionized water and 0.05 g $\text{C}_{12}\text{H}_{22}\text{O}_{11}$ as a green capping agent was added slowly into the mixture at 50°C and 400 rpm for 45 minutes. For growth and initial nucleation, this solution was exposed to ultrasonic irradiation at 20 kHz with a maximum power output of 60 W. Finally, both solutions were transferred to a beaker

and the mixture was exposed to a hydrothermal steel reactor at different temperatures and times. In the final step, the white precipitate was centrifuged at 4000 rpm for 10 minutes and collected by filter paper washed with ethanol and dried at room temperature for 48 hours. The as-prepared products were analyzed by XRD, EDAX, SEM, TEM and FT-IR.

Preparation of Agar Cultivation

To prepare ten consecutive dilutions, at first 4.6 mg of the $\text{La}^{3+}/\alpha\text{-Al}_2\text{O}_3$ NPs as-synthesized compounds were dissolved with a minimum amount of dimethyl sulfoxide (DMSO) and distilled water to a volume of 5 mL to a storage concentration of 1280 $\mu\text{g}/\text{mL}$, then with consecutive dilutions the concentrations were obtained from the sample. For this purpose, 10 small tubes were filled with 2 mL of the Muller-Hinton broth, then 10 large tubes (25 mL) were filled with 18 mL of the Muller-Hinton agar and transferred to the autoclave. In the next step, the first tube was added to 2 mL of the stock solution and after mixing, 2 mL of the first tube was added to the second tube. This process proceeded in the same way, until finally, 2 cc of the final tube were poured out and 8 consecutive dilutions were prepared from the specimen and concentrations of 640, 320, 160, 80, 40, 20, 10 and 5 $\mu\text{g}/\text{mL}$ were obtained. Each of these dilutions was then added to 18 cc of solid culture medium and the final concentrations were achieved as 64, 32, 16, 8, 4, 2, 1 and 0.5 $\mu\text{g}/\text{mL}$.

Experimental Design

Factorial designs are primarily used to screen significant factors.²² To synthesize $\text{La}^{3+}/\alpha\text{-Al}_2\text{O}_3$ nanoparticles, the $2k^{-1}$ factorial method was utilized to evaluate the effects of the parameters such as hydrothermal time, temperature, ultrasound irradiation power and interaction between these factors on the properties of the $\text{La}^{3+}/\alpha\text{-Al}_2\text{O}_3$ nanoparticles. As can be seen from factorial designs, under different synthesis conditions, including hydrothermal time, temperature, and ultrasound irradiation power, $\text{La}^{3+}/\alpha\text{-Al}_2\text{O}_3$ nanoparticles had different particle size distributions. The results demonstrated that a total of two factors, hydrothermal time and temperature, had the greatest impact on the size of nanoparticles. Figure 1 shows the normal plot of the effects, the Pareto chart, contour plot of size and surface plot of hydrothermal time vs temperature and size (nm).

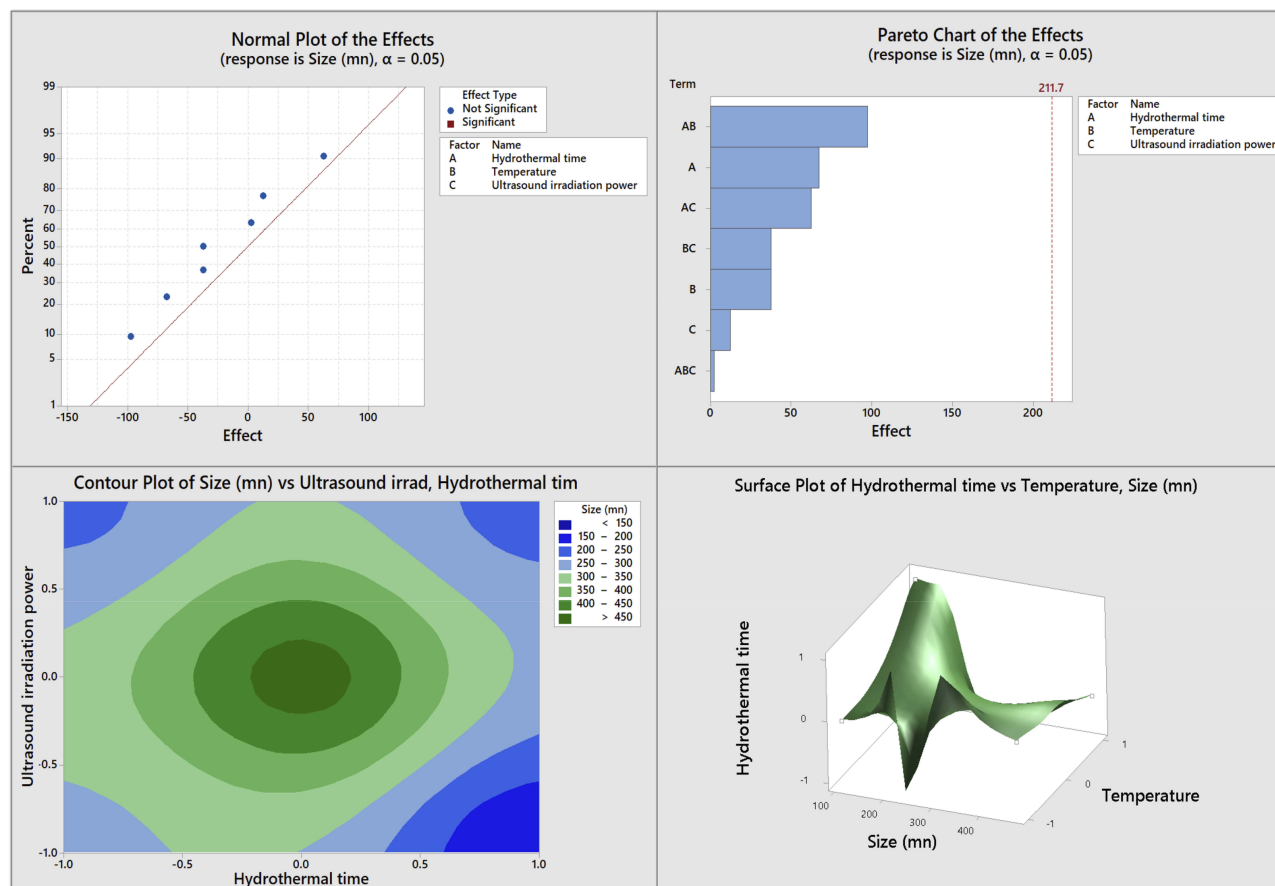


Figure 1 Data of factorial design as hydrothermal time, temperature, ultrasound irradiation power and interaction between these factors by the size (nm).

Results and Discussion

Characterization of $\text{La}^{3+}/\alpha\text{-Al}_2\text{O}_3$ Nanoparticles

In this study, we used the fructose as a green capping agent with ultrasonic-assisted microwave technology with high efficiency for the synthesis of $\text{La}^{3+}/\alpha\text{-Al}_2\text{O}_3$ nanoparticles. X-Ray Diffraction analysis (XRD) as a rapid analytical technique was used for phase identification of crystalline material. Figure 2 shows the XRD patterns of the $\alpha\text{-Al}_2\text{O}_3$ NPs (JCPDS No.01-0287) and the $\text{La}^{3+}/\alpha\text{-Al}_2\text{O}_3$ NPs as-synthesized samples obtained in the presence of the fructose at room temperature and calcined at 300°C . The fructose concentration plays a key role in the formation of the $\text{La}^{3+}/\alpha\text{-Al}_2\text{O}_3$ (JCPDS No.04-0858) when the fructose concentrations were 1.5 mol/L. To characterize phases and examine crystallite size of the $\text{La}^{3+}/\alpha\text{-Al}_2\text{O}_3$ NPs, we used the Sherrer equation (Equation 1 to calculate the mean diameter and the crystallographic properties with the help of the following formula):³⁶

$$D = k\lambda/\beta\cos(\theta) \quad (1)$$

In this equation, D is the mean crystallites size, λ is the X-ray wavelength (1.54056 \AA), β is the broadening of the

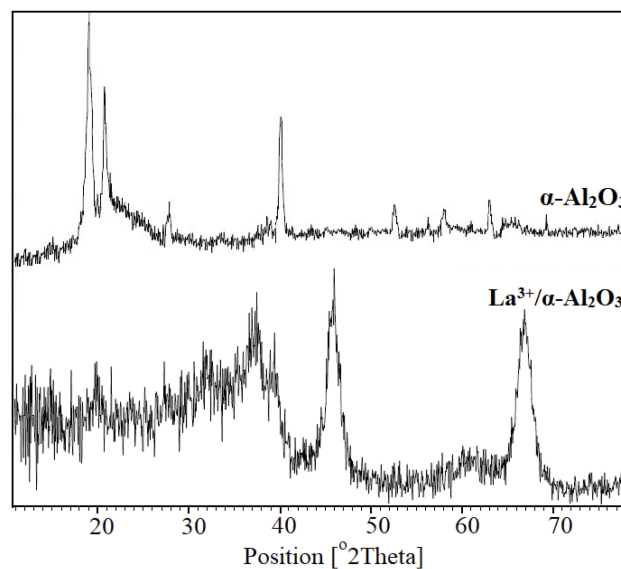


Figure 2 XRD patterns of the $\alpha\text{-Al}_2\text{O}_3$ NPs and the as-synthesized $\text{La}^{3+}/\alpha\text{-Al}_2\text{O}_3$ NPs heating after calcination at 300°C for 3 hours.

line measured at half its maximum intensity (in radius), θ is the diffraction angle from Bragg planes and k is the shape factor (0.9).

Thus, it can be inferred that $\text{La}^{3+}/\alpha\text{-Al}_2\text{O}_3$ nanocomposite was successfully synthesized. Figure 3A and B show the SEM and TEM images of the samples prepared via the ultrasound-

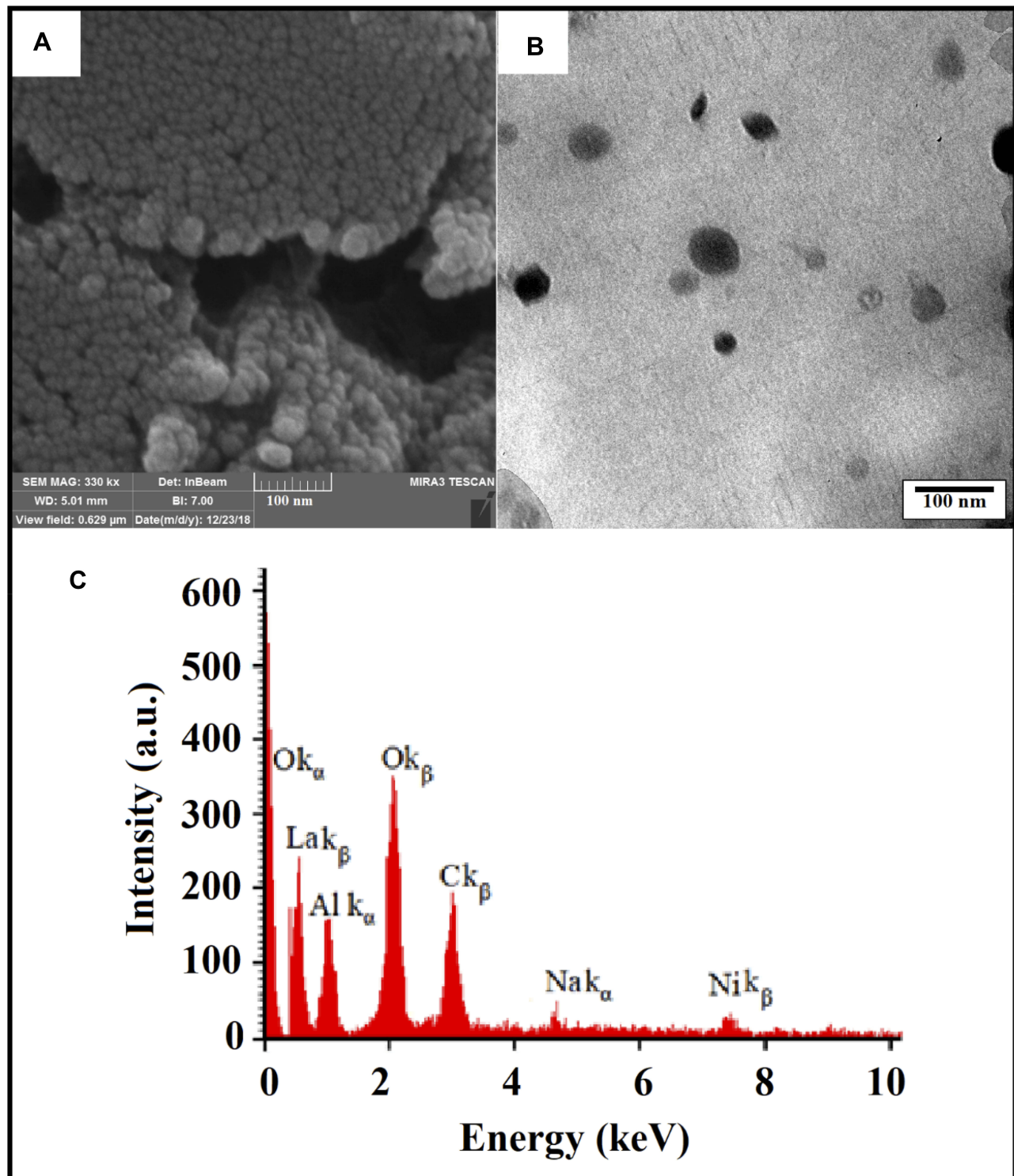


Figure 3 The SEM image (A), TEM image (B) and electron dispersive spectroscopy (EDX) (C) as-synthesized $\text{La}^{3+}/\alpha\text{-Al}_2\text{O}_3$ NPs prepared via ultrasound assisted hydrothermal method.

assisted hydrothermal method, respectively. The results show that some small round particles having more uniform size and shape were located together. Owing to the high surface area of the $\text{La}^{3+}/\alpha\text{-Al}_2\text{O}_3$, nanocomposites tend to agglomerate together. For this reason, in producing the samples, we used the Cetyltrimethyl ammonium Bromide (CTAB) reagent as surfactant which led to increasing stability of the small particles and prevention of aggregations. The microscopic analysis fully demonstrates which components in $\text{La}^{3+}/\alpha\text{-Al}_2\text{O}_3$ nanocomposites are in close contact with each other and are sufficiently dispersed, thereby indicating that the products have been produced successfully. Briefly, this analysis showed that the nanocomposites had homogenous sphere morphology and did not produce aggregated structures. The particle sizes visualized in the TEM images corroborated with the nanocomposites sizes were obtained by SEM. To further validate the as-synthesized $\text{La}^{3+}/\alpha\text{-Al}_2\text{O}_3$ nanocomposites, electron dispersive spectroscopy was applied (Figure 3C). The results demonstrate La: Al: O elements as elemental composition of $\text{La}^{3+}/\alpha\text{-Al}_2\text{O}_3$ nanocomposites. The presence of the C element is related to CTAB, which is used as the surfactant and distribution of the particle size.

The EDS and elemental mapping depict the presence of La, Al, O and C elements as the principal elements of the nanocomposite. Both techniques clearly show the $\text{La}^{3+}/\alpha\text{-Al}_2\text{O}_3$ nanocomposites synthesized successfully using the ultrasound-assisted hydrothermal method Figure 4A.

The ultraviolet–visible spectroscopy of the $\text{La}^{3+}/\alpha\text{-Al}_2\text{O}_3$ nanocomposite was further studied under an excitation wavelength ranging from 190 nm to 260 nm which is shown in Figure 4B. The fluorescence intensity could reflect the photo charges separation rate of the as-prepared photo catalysts, and lower intensity corresponds to higher photo charges separation rate and transportation. As Figure 4B displays, emission peaks located at approximately 220 nm, 215 nm, 211 nm and 205 nm were clearly shown for samples S1–S4. It can be concluded that at a constant temperature with increasing time from 4 hours up to 10 hours, the size of the nanostructures gradually increases and blueshift can occur. Figure 4B shows the UV-vis spectra of as-synthesized $\text{La}^{3+}/\alpha\text{-Al}_2\text{O}_3$ NPs under different conditions such as 10 hours (S1), 8 hours (S2), 6 hours (S3), and 4 hours (S4) at 200°C.

To determine the structural properties of the synthesized $\text{La}^{3+}/\alpha\text{-Al}_2\text{O}_3$ nanocomposites were subjected with Fourier-transform infrared spectroscopy (FT-IR). Overall, the reactions expected for synthesized $\text{La}^{3+}/\alpha\text{-Al}_2\text{O}_3$ nanocomposites were as follows (Equation 2–4):

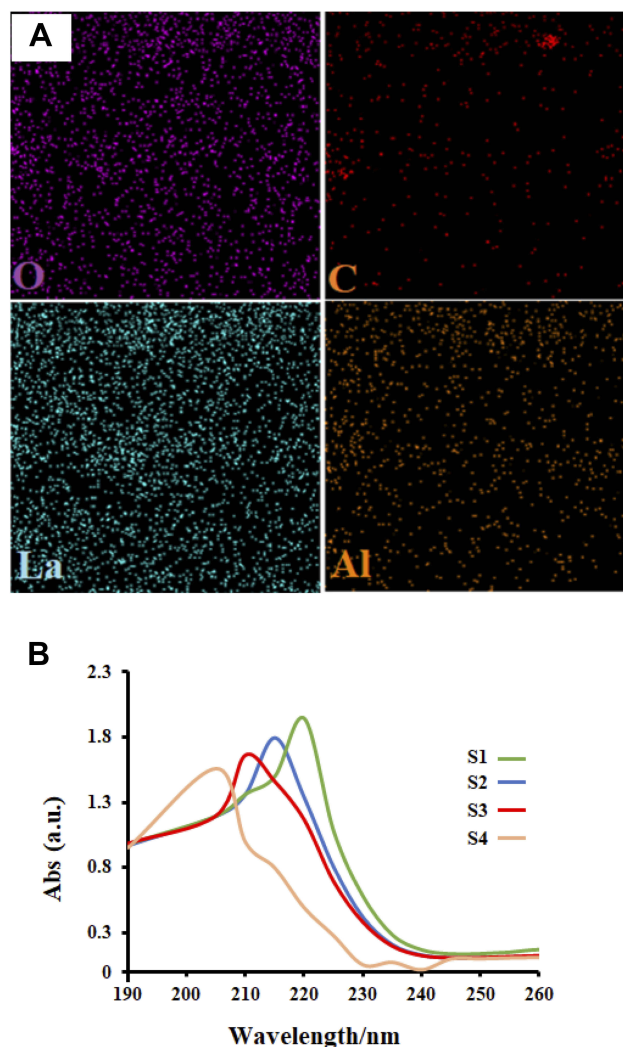


Figure 4 Elemental mapping analysis of the as-synthesized $\text{La}^{3+}/\alpha\text{-Al}_2\text{O}_3$ NPs (A) and the UV-vis spectra of the as synthesized $\text{La}^{3+}/\alpha\text{-Al}_2\text{O}_3$ NPs in different conditions such as 10 hours (S1), 8 hours (S2), 6 hours (S3), and 4 hours (S4) at 200°C (B).

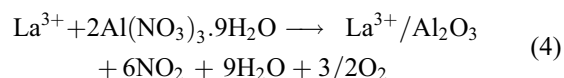
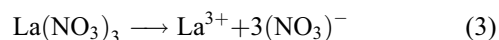
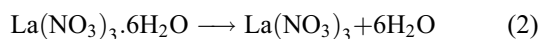


Figure 5A and B show the FT-IR spectrum at 400–4000 cm^{-1} for $\alpha\text{-Al}_2\text{O}_3$ and $\text{La}^{3+}/\alpha\text{-Al}_2\text{O}_3$ nanocomposites as-synthesized after 300°C, respectively. The results indicate that the bands centered at 500–900 cm^{-1} are related to metal–oxygen. A wide peak centered at 3450 cm^{-1} can be attributed to the stretching vibration of the O–H band of H_2O molecules. Owing to the high surface to volume ratio of the nanostructures, products can adsorb more O–H molecules on their surfaces than the bulk ones. The broad absorption peak

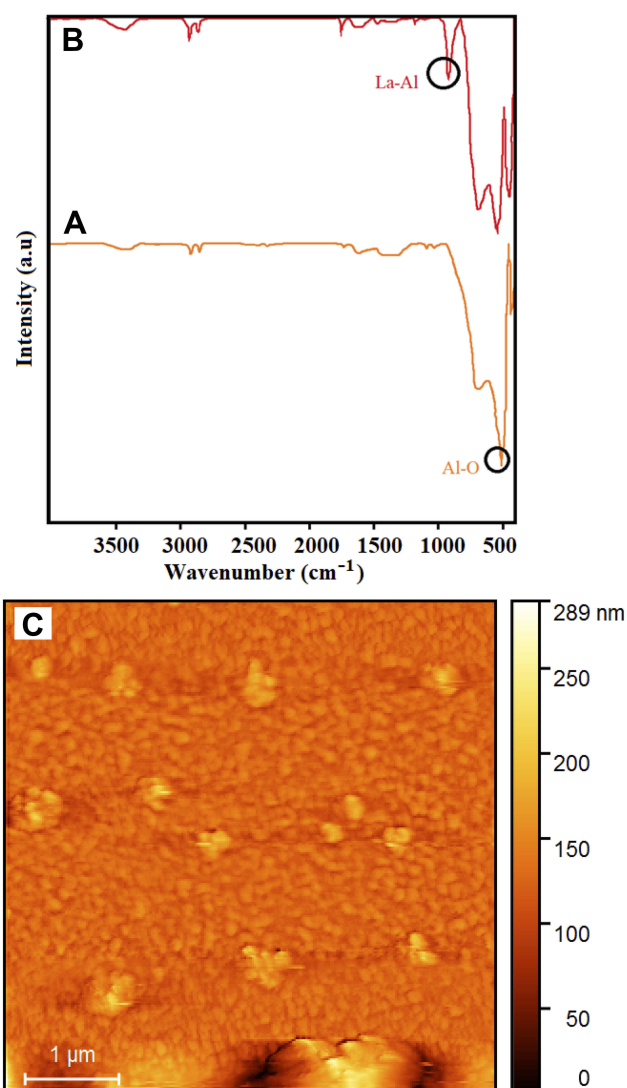


Figure 5 The FT-IR spectrum of the α -Al₂O₃ (A), La³⁺/ α -Al₂O₃ nanocomposites as-synthesized after 300°C (B) and AFM images of the La³⁺/ α -Al₂O₃ nanocomposites after annealing at 200°C for 6 hours (C).

at 985–990 cm⁻¹ range matches La-Al bands, being mainly related to La-Al-O bands in La³⁺/ α -Al₂O₃ network structures. The Atomic Force Microscopy (AFM) images of the La³⁺/ α -Al₂O₃ nanocomposites displayed the narrow and regular form together. The roughness and surface properties of the final products can be calculated with the root mean-squared roughness (RMS) as a factor obtained from the standard deviation of the AFM image data and determined according to the following equation (Equation 5):

$$R_{rms} = \sqrt{\frac{\sum_{n=1}^N (z_n - \bar{z})^2}{N - 1}} \quad (5)$$

In this equation, z_n represents the height of the n^{th} data, \bar{z} is equal to the mean height of Z_n in AFM topography, and

N is the number of data. For an area of 87.22 pm², the roughness average is 96.32 nm. Figure 5C shows the AFM topography images of La³⁺/ α -Al₂O₃ nanocomposites.

Figure 6A presents the Brunauer–Emmett–Teller (BET) surface area measurement using the N₂ adsorption/desorption isotherm data of the La³⁺/ α -Al₂O₃ nanocomposites. Also the distribution of the pores appears multi-peak for the as-synthesized La³⁺/ α -Al₂O₃ nanocomposites at 300°C shown in Figure 6B. The results indicate porosity in the samples at room temperature to 800°C in the airflow of 10 cm³ min⁻¹.

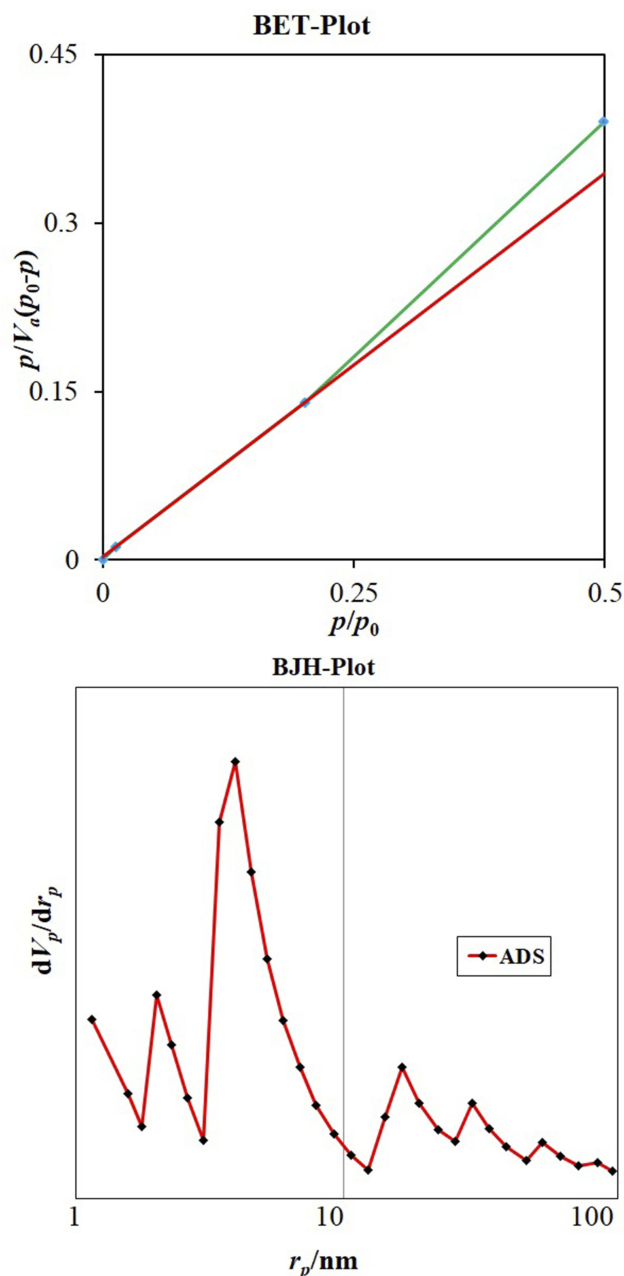


Figure 6 The N₂ adsorption/desorption isotherm (A) and pore size distribution curve data of the La³⁺/ α -Al₂O₃ nanocomposites (B).

Table 1 presents a summary of all experimental parameters of BET surface area analysis such as pore volume (cm^3/g), and pore diameter (nm). The findings through the BJH (Barret–Joyner–Halenda) method demonstrate that $\text{La}^{3+}/\alpha\text{-Al}_2\text{O}_3$ nanocomposites have high porosity. Moreover, the adsorption/desorption isotherm data such as cross section area, total pore volumes and dead volume as 0.175 (nm^2), 0.0359 (cm^3g^{-1}) and 17.909 (cm^3) were obtained, respectively. Also, the average pore diameter was calculated as 25.67 nm using BET isotherm data.

Antimicrobial Effect of $\text{La}^{3+}/\alpha\text{-Al}_2\text{O}_3$

In this study, the agar well diffusion assay was used to evaluate the antimicrobial activity of $\text{La}^{3+}/\alpha\text{-Al}_2\text{O}_3$ nanocomposites, and prevention of bacterial growth was determined in the culture media loaded with different concentrations of nanocomposites such as 64, 32, 16, 8, 4, 2, 1, and 0.5 $\mu\text{g}/\text{mL}$. To determine the non-contamination of the culture medium, a tube containing a culture medium without specimens and a microbe were considered a negative control. Furthermore, to detect the lack of antimicrobial activity, the medium was cultured from a tube containing culture medium and a non-sampled bacterium as a positive control. To detect antimicrobial insufficiency and ensure the uniform growth of bacteria on a plate surface of the solvent, positive control and a negative control of the culture medium and the solvent and the microbial strain for dimethyl sulfoxide

Table 1 The Surface Features of the $\text{La}^{3+}/\alpha\text{-Al}_2\text{O}_3$ Nanocomposites as-synthesized after 300°C

BET area ($\text{m}^2 \text{g}^{-1}$)	Pore volume ($\text{cm}^3 \text{g}^{-1}$)	Pore diameter (nm)
37.879	0.359	22.679

were considered. Each plate was studied in terms of growth and non-growth of tested microorganisms. Gram-negative and Gram-positive bacteria showed a higher sensitivity to $\text{La}^{3+}/\alpha\text{-Al}_2\text{O}_3$ nanocomposites at the lower concentration. Table 2 shows the MIC method for antibacterial activity within the range of 0.5 – 64 $\mu\text{g}/\text{mL}$.

As the results show, all of the bacterial strains showed maximum sensitivity to different concentrations of $\text{La}^{3+}/\alpha\text{-Al}_2\text{O}_3$ nanocomposites but among bacterial strains *M. luteus* PTCC. 1110 showed growth in 4 $\mu\text{g}/\text{mL}$. Antibacterial activity of $\text{La}^{3+}/\alpha\text{-Al}_2\text{O}_3$ nanocomposites against 4 Gram-negative and 4 Gram-positive bacteria using agar well diffusion with nanocomposites prepared under different conditions as 64, 32, 16, 8, 4, 2, 1, 0.5 $\mu\text{g}/\text{mL}$ in solid culture mediums from 1 to 8 respectively are shown in Figure 7. The results show that *M. luteus* PTCC. 1110 has an inhibition zone in the concentration of $\text{La}^{3+}/\alpha\text{-Al}_2\text{O}_3$ nanocomposites within 4 – 0.5 $\mu\text{g}/\text{mL}$. The zone of inhibition observed for this bacterial strain is lower than that of all the bacteria studied for the same loading of nanoparticles. The goal of this study is to use honey as a natural reagent also as a biomolecules template, green reductant and capping agent for the synthesized $\text{La}^{3+}/\alpha\text{-Al}_2\text{O}_3$ nanocomposites. The $\text{La}^{3+}/\alpha\text{-Al}_2\text{O}_3$ nanocomposites with thiol groups of enzymes that could be through the release of oxygen species, disrupted their respiratory chains. Therefore, damage occurred in the cell structures and finally led to cell death mechanism.

Conclusion

This present study deals with synthesis, characterization and antibacterial activity of particle-linked $\text{La}^{3+}/\alpha\text{-Al}_2\text{O}_3$ nanocomposites. The $\text{La}^{3+}/\alpha\text{-Al}_2\text{O}_3$ was synthesized with the ultrasonic-assisted hydrothermal method in the presence of honey as an ecofriendly and natural reagent.

Table 2 Antibacterial Activity of the $\text{La}^{3+}/\alpha\text{-Al}_2\text{O}_3$ Nanocomposites with MIC ($\mu\text{g}/\text{mL}$) Method Against Selected Gram-Positive and Gramnegative Pathogenic Bacterial Strains

Concentration ($\mu\text{g}/\text{mL}$)	64 $\mu\text{g}/\text{mL}$	32 $\mu\text{g}/\text{mL}$	16 $\mu\text{g}/\text{mL}$	8 $\mu\text{g}/\text{mL}$	4 $\mu\text{g}/\text{mL}$	2 $\mu\text{g}/\text{mL}$	1 $\mu\text{g}/\text{mL}$	0.5 $\mu\text{g}/\text{mL}$
Bacteria								
<i>E. coli</i> PTCC 1330	-	-	-	-	-	-	-	-
<i>K. pneumoniae</i> PTCC 1053	-	-	-	-	-	-	-	-
<i>S. marcescens</i> PTCC1621	-	-	-	-	-	-	-	-
<i>P. aeruginosa</i> PTCC1074	-	-	-	-	-	-	-	-
<i>S. aureus</i> PTCC. 1112	-	-	-	-	-	-	-	+
<i>M. luteus</i> PTCC. 1110	-	-	-	-	+	+	+	+
<i>B. subtilis</i> PTCC. 1023	-	-	-	-	-	-	-	-
<i>S. epidermidis</i> PTCC 1114	-	-	-	-	-	-	-	-

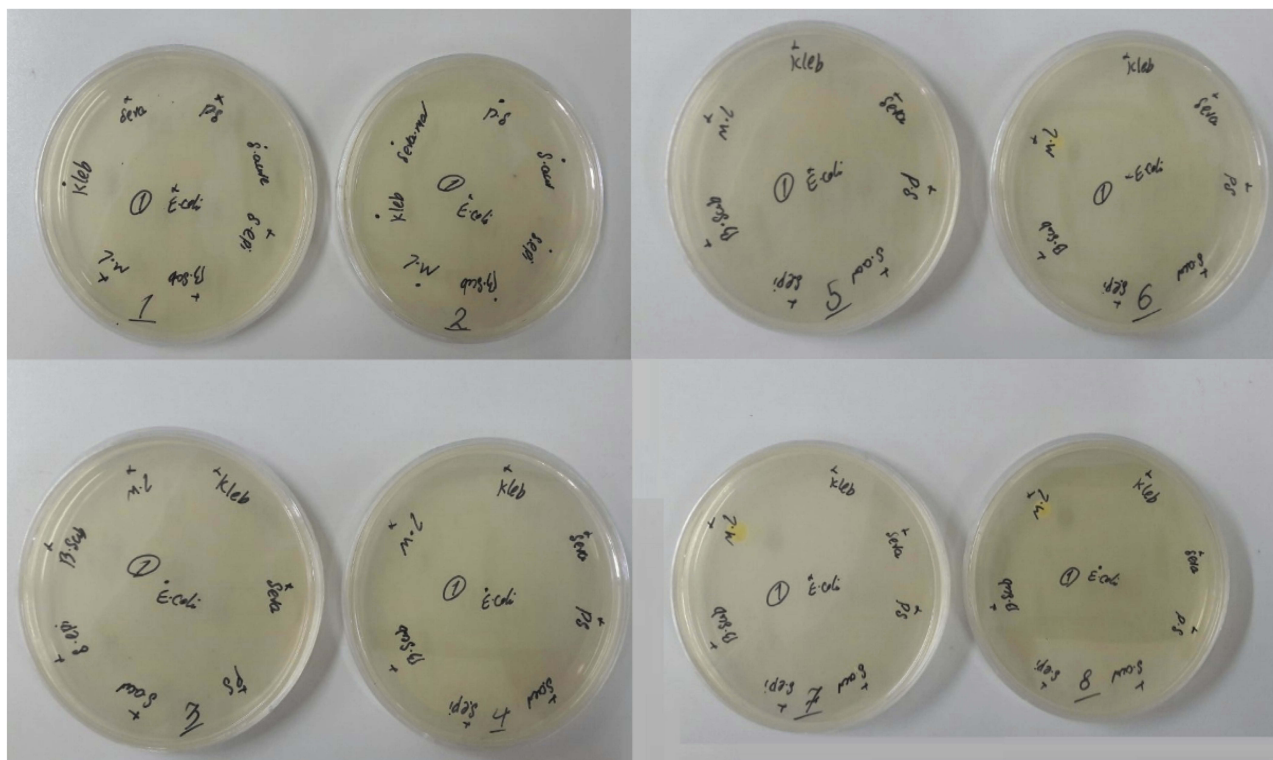


Figure 7 Antibacterial activity of $\text{La}^{3+}/\alpha\text{-Al}_2\text{O}_3$ nanocomposites against 4 gram-negative and 3 gram-positive bacteria. Different serial dilutions were 64 (plate 1), 32 (plate 2), 16 (plate 3), 8 (plate 4), 4 (plate 5), 2 (plate 6), 1 (plate 7) and 0.5 (plate 8) $\mu\text{g/mL}$ of the $\text{La}^{3+}/\alpha\text{-Al}_2\text{O}_3$ nanocomposites which added to the Mueller-Hinton agar medium.

Based on the obtained results, it was found that $\text{La}^{3+}/\alpha\text{-Al}_2\text{O}_3$ nanocomposites showed suitable antibacterial effects on some pathogenic microbial strains. Our results demonstrate that the use of glucose as a green capping and reductant agent as well as an eco-friendly, simple, nontoxic pathway can lead to producing nanostructures with the suitable size distribution.

Research Highlights

- Sphere like $\text{La}^{3+}/\alpha\text{-Al}_2\text{O}_3$ nanocomposites were synthesized in an ecofriendly way with the ultrasound-assisted hydrothermal method.
- Honey as a natural reagent was used in the synthesis of $\text{La}^{3+}/\alpha\text{-Al}_2\text{O}_3$ nanocomposites.
- The $\text{La}^{3+}/\alpha\text{-Al}_2\text{O}_3$ nanoparticles show high efficiency antimicrobial properties for pathogenic microbial strains.
- The $\text{La}^{3+}/\alpha\text{-Al}_2\text{O}_3$ nanoparticles show an excellent antibacterial activity.

Acknowledgments

The authors are grateful to the council of the Pharmaceutics Research Center, Institute of Neuropharmacology, Kerman University of Medical Sciences, Kerman, Iran.

Disclosure

The authors declare that they have no conflicts of interest in this work.

References

- Das D, Nath BC, Phukon P, et al. Synthesis and evaluation of antioxidant and antibacterial behavior of CuO nanoparticles. *Colloids Surf.* 2013;101:430–433. doi:10.1016/j.colsurfb.2012.07.02
- Balasoorya ER, Jayasinghe CD, Jayawardena UA, Ruwanthika RW, Mendis de Silva R, Udagama PV. Honey mediated green synthesis of nanoparticles: new era of safe nanotechnology. *J Nanomater.* 2017;2017.
- Hashemi Gahrue H, Niakousari M. Antioxidant, antimicrobial, cell viability and enzymatic inhibitory of antioxidant polymers as biological macromolecules. *Int J Biol Macromol.* 2017;104:606–617. doi:10.1016/j.ijbiomac.2017.06.021
- Zhong D, Liu Y, Liao X, et al. Facile preparation of binder-free NiO/MnO₂-carbon felt anode to enhance electricity generation and dye wastewater degradation performances of microbial fuel cell. *Int J Hydrogen Energy.* 2018;43(51):23014–23026. doi:10.1016/j.ijhydene.2018.10.144
- Patil MP, Kim G-D. Marine microorganisms for synthesis of metallic nanoparticles and their biomedical applications. *Colloids Surf.* 2018;172:487–495. doi:10.1016/j.colsurfb.2018.09.007
- Rivera-Rangel RD, González-Muñoz MP, Avila-Rodríguez M, et al. Green synthesis of silver nanoparticles in oil-in-water microemulsion and nano-emulsion using geranium leaf aqueous extract as a reducing agent. *Colloids Surf A.* 2018;536:60–67. doi:10.1016/j.colsurfa.2017.07.051

7. Rosa M, Gooden PN, Butterworth S, et al. Zirconia nano-colloids transfer from continuous hydrothermal synthesis to inkjet printing. *J Eur Ceram Soc.* 2019;39(1):2–8. doi:10.1016/j.jeurceramsoc.2017.11.035
8. Zare N, Zabardasti A, Mohammadi A, et al. Synthesis of spherical Fe₂O₃ nanoparticles from the thermal decomposition of iron (III) nano-structure complex: DFT studies and evaluation of the biological activity. *Bioorg Chem.* 2018;80:334–346. doi:10.1016/j.bioorg.2018.07.005
9. Zhang D, Deng X, Zhang Q, et al. Design and synthesis of ruthenium nanoparticles on polyanilines (nano Ru@PANIs) via Ru-catalyzed aerobic oxidative polymerization of anilines. *Mater Lett.* 2019;234:216–219. doi:10.1016/j.matlet.2018.09.108
10. Çevik A, Alzebaree R, Humur G, et al. Effect of nano-silica on the chemical durability and mechanical performance of fly ash based geopolymer concrete. *Ceram Int.* 2018;44(11):12253–12264. doi:10.1016/j.ceramint.2018.04.009
11. Fan G, Bao M, Zheng X. Growth inhibition of harmful cyanobacteria by nanocrystalline Cu-MOF-74: efficiency and its mechanisms. *J Hazard Mater.* 2018;367:529–538.
12. Bao Q, Zhu W, Yan J, et al. Vapor phase aldol condensation of methyl acetate with formaldehyde over a Ba–La/Al₂O₃ catalyst: the stabilizing role of La and effect of acid–base properties. *RSC Adv.* 2017;7(82):52304–52311. doi:10.1039/C7RA10008F
13. Khatamian M, Khandar AA, Divband B, et al. Heterogeneous photocatalytic degradation of 4-nitrophenol in aqueous suspension by Ln (La³⁺, Nd³⁺ or Sm³⁺) doped ZnO nanoparticles. *J Mol Catal.* 2012;365:120–127. doi:10.1016/j.molcata.2012.08.018
14. Sanad M, Rashad MM, Abdel-Aal EA, et al. Effect of Y³⁺, Gd³⁺ and La³⁺ dopant ions on structural, optical and electrical properties of o-mullite nanoparticles. *J Rare Earths.* 2014;32(1):37–42. doi:10.1016/S1002-0721(14)60031-4
15. Ponnillavan V, Vasanthavel S, Singh RK, et al. Influence of La³⁺ additions on the phase behaviour and antibacterial properties of ZrO₂–SiO₂ binary oxides. *Ceram Int.* 2015;41(6):7632–7639. doi:10.1016/j.ceramint.2015.02.089
16. Singh R, Nalwa HS. Medical applications of nanoparticles in biological imaging, cell labeling, antimicrobial agents, and anticancer nanodrugs. *J Biomed Nanotechnol.* 2011;7(4):489–503. doi:10.1166/jbn.2011.1324
17. Verdiá-Báguena C, Queralt-Martín M, Aguilera VM, et al. Protein ion channels as molecular ratchets. switchable current modulation in outer membrane protein f porin induced by millimolar La³⁺ ions. *J Phys Chem C.* 2012;116(11):6537–6542. doi:10.1021/jp210790r
18. Preethi J, Meenakshi S. Fabrication of La³⁺ impregnated chitosan/β-cyclodextrin biopolymeric materials for effective utilization of chromate and fluoride adsorption in single systems. *J Chem Eng Data.* 2018;63(3):723–731. doi:10.1021/acs.jced.7b00889
19. Kumar L, Kar M. Effect of La³⁺ substitution on the structural and magnetocrystalline anisotropy of nanocrystalline cobalt ferrite (CoFe₂–xLa_xO₄). *Ceram Int.* 2012;38(6):4771–4782. doi:10.1016/j.ceramint.2012.02.065
20. Michau TM, Davidson MG, Gilger BC. Carbon dioxide laser photobleaching adjunctive therapy following superficial lamellar keratectomy and bulbar conjunctivectomy for the treatment of corneolimbic squamous cell carcinoma in horses: a review of 24 cases. *Vet Ophthalmol.* 2012;15(4):245–253. doi:10.1111/vop.2012.15.issue-4
21. Zhu S, Meng Q, Wang L, et al. Highly photoluminescent carbon dots for multicolor patterning, sensors, and bioimaging. *Angewandte Chemie.* 2013;125(14):4045–4049. doi:10.1002/ange.v125.14
22. Huang Y, Coman D, Ali MM, et al. Lanthanide ion (III) complexes of 1, 4, 7, 10-tetraazacyclododecane-1, 4, 7, 10-tetraaminophosphonate for dual biosensing of pH with chemical exchange saturation transfer (CEST) and biosensor imaging of redundant deviation in shifts (BIRDS). *Contrast Media Mol Imaging.* 2015;10(1):51–58. doi:10.1002/cmmi.v10.1
23. Li C, Yang J, Yang P, et al. Hydrothermal synthesis of lanthanide fluorides LnF₃ (Ln= La to Lu) nano-/microcrystals with multiform structures and morphologies. *Chem Mater.* 2008;20(13):4317–4326. doi:10.1021/cm800279h
24. Fang Y-P, Xu A-W, Song R-Q, et al. Systematic synthesis and characterization of single-crystal lanthanide orthophosphate nanowires. *J Am Ceram Soc.* 2003;125(51):16025–16034. doi:10.1021/ja037280d
25. Dizaj SM, Lotfipour F, Barzegar-Jalali M, et al. Antimicrobial activity of the metals and metal oxide nanoparticles. *Mater Sci Eng.* 2014;44:278–284. doi:10.1016/j.msec.2014.08.031
26. Lakshmi SD, Avti PK, Hegde G. Activated carbon nanoparticles from biowaste as new generation antimicrobial agents: a review. *Nano-Struct Nano-Objects.* 2018;16:306–321. doi:10.1016/j.nanoso.2018.08.001
27. Raghunath A, Perumal E. Metal oxide nanoparticles as antimicrobial agents: a promise for the future. *Int J Antimicrob Agents.* 2017;49(2):137–152. doi:10.1016/j.ijantimicag.2016.11.011
28. Rodrigues GR, López-Abarrategui C, de la Serna Gómez I, et al. Antimicrobial magnetic nanoparticles based-therapies for controlling infectious diseases. *Int J Pharm.* 2019;555:356–367. doi:10.1016/j.ijpharm.2018.11.043
29. Amist N, Singh NB, Yadav K, et al. Comparative studies of Al³⁺ ions and Al₂O₃ nanoparticles on growth and metabolism of cabbage seedlings. *J Biotechnol.* 2017;254:1–8. doi:10.1016/j.jbiotec.2017.06.002
30. Atzenhofer C, Gschiel S, Harmuth H. Phase formation in Al₂O₃-C refractories with Al addition. *J Eur Ceram Soc.* 2017;37(4):1805–1810. doi:10.1016/j.jeurceramsoc.2016.11.027
31. Oliveira RS, Machado PMA, Ramalho HF, et al. Acylation of epoxidized soybean biodiesel catalyzed by SnO/Al₂O₃ and evaluation of physical chemical and biologic activity of the product. *Ind Crops Prod.* 2017;104:201–209. doi:10.1016/j.indcrop.2017.04.049
32. Bentancor M, Vidal S. Programmable and low-cost ultraviolet room disinfection device. *HardwareX.* 2018;4:e00046. doi:10.1016/j.ohx.2018.e00046
33. Ponnachan P, Vinod V, Pullanhi U et al. Antifungal activity of octenidine dihydrochloride and ultraviolet-C light against multidrug-resistant *Candida auris*. *J Hosp Inf.* 2018;102:120–124.
34. Zhong F, Xu M, Schelli K, et al. Comparing the impact of ultrafine particles from petrodiesel and biodiesel combustion to bacterial metabolism by targeted HPLC-MS/MS metabolic profiling. *Ecotoxicol Environ Saf.* 2017;142:164–170. doi:10.1016/j.ecoenv.2017.04.002
35. Zotin AA, Pokrovskii VN. The growth and development of living organisms from the thermodynamic point of view. *Phys A.* 2018;512:359–366. doi:10.1016/j.physa.2018.08.094
36. Moosavi S, Zakaria S, Chia CH, et al. Hydrothermal synthesis, magnetic properties and characterization of CoFe₂O₄ nanocrystals. *Ceram Int.* 2017;43(10):7889–7894. doi:10.1016/j.ceramint.2017.03.110

International Journal of Nanomedicine

Publish your work in this journal

The International Journal of Nanomedicine is an international, peer-reviewed journal focusing on the application of nanotechnology in diagnostics, therapeutics, and drug delivery systems throughout the biomedical field. This journal is indexed on PubMed Central, MedLine, CAS, SciSearch®, Current Contents®/Clinical Medicine,

Journal Citation Reports/Science Edition, EMBase, Scopus and the Elsevier Bibliographic databases. The manuscript management system is completely online and includes a very quick and fair peer-review system, which is all easy to use. Visit <http://www.dovepress.com/testimonials.php> to read real quotes from published authors.

Submit your manuscript here: <https://www.dovepress.com/international-journal-of-nanomedicine-journal>